JOURNAL OF SPACECRAFT AND ROCKETS
Vol. 39, No. 5, September–October 2002

Resistive Deployment of Inflatable Structures Using Velcro

M. Salama,* H. Fang,† and M. Lou ‡
Jet Propulsion Laboratory, California Institute of Technology, Pasadena, California 91109

To explain the dynamics of Velcro-controlled deployment of inflatable structures, we first examine various mechanisms involved in Velcro delamination. Unlike adhesive joints, it is found that Velcro has unique characteristics, wherein multiple load-carrying mechanisms are sequentially engaged to resist separation. Both tests and analysis suggest that a strength criterion based on the strain energy density dissipated during separation can best capture these mechanisms. A finite element model of Velcro interfaces is also used, along with a finite volume inflation model, to simulate the deployment behavior of Velcro-controlled inflatable structures. Although it is essential to determine whether a selected type of Velcro will deploy, it is of equal interest to the designer to assess the rate of deployment. To this end, simulation results show that, consistent with the proposed strength criterion, the average rate of energy dissipation at the Velcro interface also seems to be the most sensitive measure of the rate of Velcro-controlled deployment.

Nomenclature

F_{analysis}	=	Velcro peeling load (analysis)
F_{av}	=	Velcro peeling load (test average)
P	=	peeling force in adhesion peeling test
r	=	radius of curvature in adhesion peeling test
T, t	=	thickness of substrate and of test strip, respectively, in adhesion peeling test
U^*	=	strain energy density
γ	=	energy of fracture/unit area of interface
γ^*	=	maximum shear strain (test)
ε^*	=	maximum normal strain (test)
σ_n	=	actual (or computed) normal stress in a general stress state
σ_s	=	actual (or computed) shear stress in a general stress state
σ^*	=	maximum normal stress (test)
τ^*	=	maximum shear stress (test)
ϕ	=	force inclination angle in peeling test

Introduction

THE stiffness and load-carrying ability of inflatable components are synonymous with their degree of inflation. This intrinsic attribute of inflatable membrane structures is particularly challenging because it attaches special significance to ensuring that the manner and sequence of their deployment is predictable, controllable, and dynamically stable. Improper deployment could result in irrecoverable entanglement of the components and possible loss of the entire mission. One way to achieve a high degree of deployment control is by providing resistive forces to counter the undesirable chaotic dynamics that may be excited by the inflation process. Two types of resistive deployment schemes have been suggested.[1,2] The first scheme is especially applicable to rolled inflatables, in which low-stiffness coil springs are embedded at selected locations in walls of the inflatable components such as tubes. The restoring torque in the coil spring provides the "muscle" required to limit the torque induced by the inflation pressure.

Received 12 June 2001; revision received 18 March 2002; accepted for publication 18 April 2002.

*Principal Engineer, Mechanical Engineering Section. Associate Fellow AIAA.
†Senior Technical Staff, Gossamer Systems Group. Member AIAA.
‡Principal Engineer, Mechanical Systems and Research Division. Associate Fellow AIAA.

In another concept, also discussed in Refs. 1 and 2, the coil springs are replaced by Velcro strips attached to the outside of interfacing walls of the inflatable membrane. In addition to being lightweight and easy to install, Velcro offers two distinct advantages over embedded springs. First, inflatable components with Velcro can be packaged by Z folding, as well as by rolling. Second, unlike coil springs, Velcro will not impose returning forces on the component being deployed after inflation deployment is completed. For these reasons, the use of Velcro is finding wide acceptance in recent inflatable designs.

To gain better understanding of the dynamic behavior of these applications, the present paper examines the mechanics of Velcro separation and its interaction with the host inflatable membrane structure. In consideration of the sparse literature on the mechanics of Velcro and the basic nature of the required information, the paper employs a combination of basic material characterization tests and analysis models and then concludes with a suitable Velcro strength criterion and a measure of the rate of Velcro-controlled deployment. The latter is particularly useful in selecting a particular Velcro strength for a given inflatable application.

Mechanics of Velcro

The interest in the use of Velcro as a structural load-carrying element is relatively new because Velcro joints are capable of carrying rather small forces. It is for this same reason, however, that Velcro is most suited for the temporary joining of the highly flexible inflatable membrane structures.

The mechanics of Velcro bonding is simple, yet its simplicity is not easily quantifiable. The bonding principle is analogous to zippers and button snaps, where adhesion occurs by mechanical interlocking of two microstructures on two corresponding mating interfaces. Applying sufficient pressure will cause a flexible microstructure on one interface to pierce and interlock with another fibrous microstructure on the mating interface. Other than the manufacturer's literature, the authors are not aware of any published investigation of Velcro bond characterization. The Velcro manufacturing process involves a large number of variables, most of which are random in nature. The variables include thickness and type of material used, the weaving/knitting fabrication technique, density of the microstructure per unit area, finishing process, type of backing, and method of attaching the Velcro system to the host products. These factors have strong influence on the manufacture's advertised Velcro strength.

The methodology used here to characterize the mechanics of Velcro follows the well-established strength of materials approach, in which we first investigate Velcro behavior under a simple stress state (such as simple tension), as well as under more complex stress states (such as under peeling loads). Then, from among the well-known strength criterion, we select one that captures Velcro separation under simple stress and that yields accurate predictions of Velcro separation under other general stress states. Analysis is used to corroborate the test results of both cases.

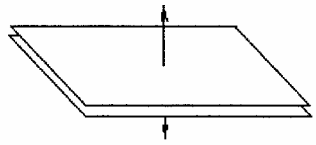

Fig. 1a Schematic unlatching tensile.

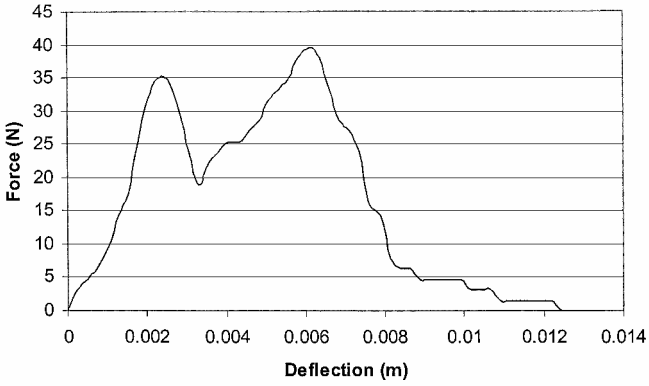

Fig. 1b Tensile force deflection for type-1 Velcro L1000-H88; strain energy = 1.86.

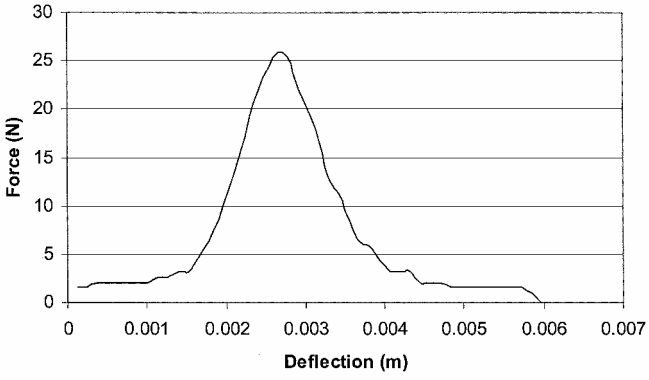

Fig. 1c Tensile force deflection for type-2 Velcro L2000-H88; strain energy = 0.367.

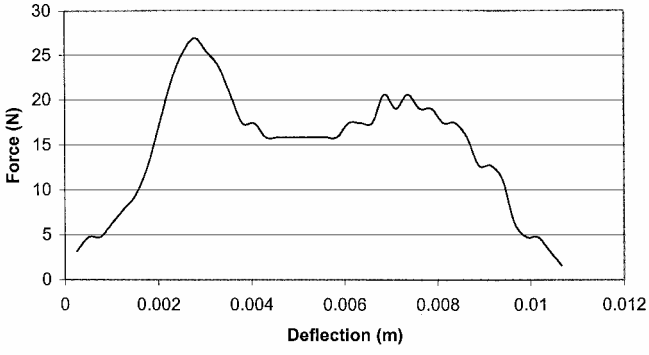

Fig. 1d Tensile force deflection for type-3 Velcro L3001-H88; strain energy = 1.38.

Velcro Behavior Under Simple Stress

The following tests were designed to characterize Velcro behavior under pure unlatching tensile stress in the direction normal to the mating interface and shear stress in the plane of the interface. Typical results from 10 tests, each for a set of pure tensile Velcro tests, are shown in Figs. 1a–1d for three types of Velcro, hereafter referred to as types 1, 2, and 3. The shear stress tests were not as repeatable as the tensile tests and are not shown here. Figures 1a–1d depict the load-deflection relationships of the three different types of Velcro from initial load application until complete separation. In two of the three types, double maximums were observed, indicating the presence of more than one load-carrying mechanism that were sequentially engaged to resist separation. The first maximum is believed to result from resistance developed within the depth of the Velcro thickness. Soon before separation, fibers near the surface were observed to engage and extend well beyond the original undeformed Velcro thickness. This second mechanism gave rise to the second maximum, which ended the last sequence of disengagements between elements of the Velcro microstructure.

Table 1 Velcro test peeling loads

Velcro peeling load	Type 1	Type 2	Type 3
F_{av}, lb (N)	1.56 (6.94)	0.95 (4.23)	1.84 (8.18)
$F_{analysis}$, lb (N)	1.59 (7.07)	0.26 (1.16)	1.60 (7.12)

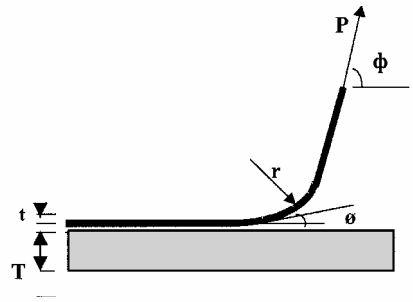

Fig. 2 Typical adhesive joint peel test.

Velcro Behavior Under Peeling

To compare with known types of bonding, adhesive joints were thought to be the closest to Velcro joints, both in configuration as well as in mechanics. To ensure adhesion of thin metallic layers to dielectric substrates, the microelectronics industry has extensively used the peel strength as an indicator of the quality of adhesive joints. Typically, the peel strength P is determined from a peel test (Fig. 2), wherein a thin strip is bonded to a rigid substrate and then pulled at some angle to measure the force that causes separation at the bond joint.

Since the first analytical investigation of the peel test by Spies,[3] many other authors[4–7] have contributed to the present-day understanding of the complex state of stress in a peel test. From these investigations of adhesive joints, we summarize findings that are relevant to the use of Velcro in controlled deployment of inflatable membranes.

First, in a typical peel test, the normal stresses at the tip of the bond interface (Fig. 2) are nearly singular and tensile, reaching about three times the yield stress. However, the stresses rapidly decrease to become slightly compressive within about t–$2t$ distance from the tip. The shear stresses there have similar singular behavior, and both normal and shear stresses die out quickly within a short distance of about $8t$ from the tip.

Second, the peel strength is strongly affected by a number of variables that relate more to the test conditions than to the actual use conditions. Most important among these are the strip thickness t; compliance of the substrate; and the test configuration reflected by r, ϕ, and Φ in Fig. 2.

Third, when peeling is in the elastic range, it has been shown that P approximates the energy of fracture γ per unit area of the interface. Otherwise, the peel strength is more of a measure of the plastic deformation there than of the interfacial fracture energy.

The load deflection relationships of Figs. 1b–1d, together with the preceding remarks, give strong indications that the mechanics of Velcro joints is different in several respects from adhesive joints. This conclusion is further investigated with the aid of the peel test configuration shown in Figs. 3a–3c, which was adapted for Velcro applications to membrane structures. The Velcro is mounted on a 0.003-in. (76.2e-06-m) thin Kapton® membrane strip, which is held fixed at the right end and then wrapped around a cylindrical drum at the left end. The drum is able to roll freely to the left as the force F applied to its axis causes the Velcro to peel at the right interface.

There were 10 peel tests performed for each of the three Velcro types corresponding to the tensile tests of Fig. 1. The average peeling load for each of the three Velcro types are summarized in the first row of Table 1.

To understand the complex state of stress during Velcro peeling, and to help correlate results of uniaxial Velcro separation with the

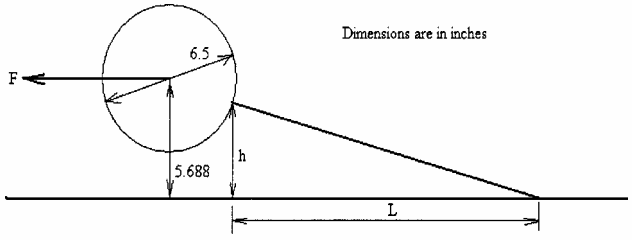

Fig. 3a Schematic of Velcro peel test.

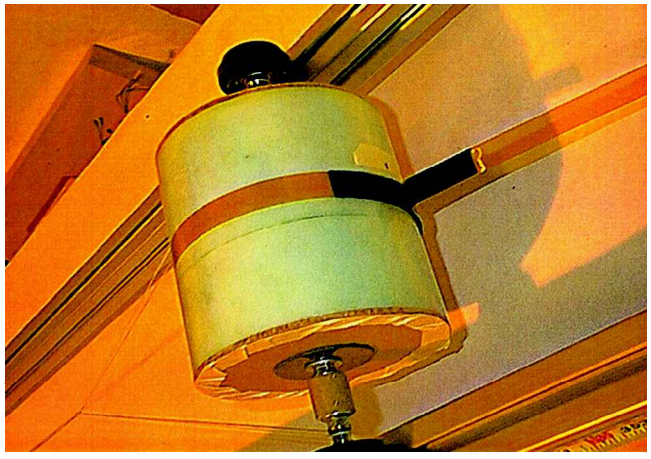

Fig. 3b Detail of Velcro peel test.

Fig. 3c Velcro separation in a peel test.

results of the peeling tests, a nonlinear finite element model was constructed to simulate the test in Fig. 3. The drum was assumed to have a linear elastic property with high rigidity. The Kapton strip with dimensions 0.75 in. (0.019 m) wide and 0.003 in. (76.2*e*-06 m) thick is modeled as capable of linear elasticity and large deformation. The Velcro joint, however, was modeled by a row of nonlinear spring elements, each capable of large deformation, as well as of a nonlinear force–displacement relationship that followed the test-derived curves of Fig. 1. As such, the force F (Fig. 3a) is applied in small incremental steps using modified Newton–Raphson iterations until separation is detected.

The forces resulting in interface separation are summarized in the second row of Table 1 for the three Velcro types. Except for type 2, the correlation between the analytical simulation and actual tests is rather good. A qualitative description of the propagation of load distribution in the Velcro at the onset and succeeding stages of peeling is given by the three snap shots of animation in Fig. 4. Well before separation, stresses start to build up near the tip until they reach some maximum value. The load is then partially transferred to the contiguous microstructure as a stress wave with two peaks, resembling the uniaxial load-deflection curves of Fig. 1. The ability of Velcro to redistribute the loads internally is believed to be due to

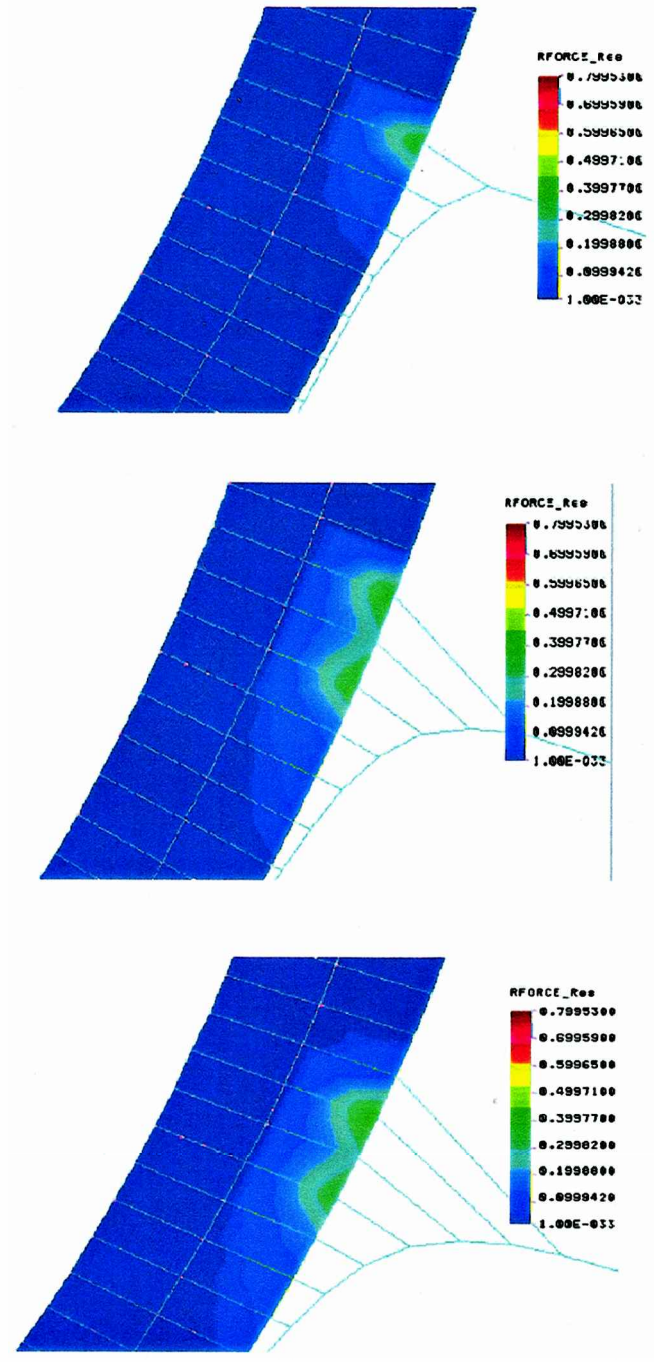

Fig. 4 Propagation of stress waves and load redistribution during Velcro peeling.

the presence of multiple load-resisting mechanisms. This contrasts the behavior of adhesive joints, where nearly singular stresses are found at the tip of adhesive joints.

Velcro Strength Criterion

Examination of results of the Velcro uniaxial tests and the peel tests reveals that the magnitude of the maximum load for each of the three Velcro types (Fig. 1) cannot explain by itself their ability to carry different peeling loads (Table 1). However, the total strain energy represented by the area under the curve (Fig. 1) seems to be much more consistent with the trend in variations in the peeling load. On the basis of this observation, we postulate that, under any stress state, Velcro separation will ensue if the strain energy density (strain energy per unit Velcro area) reaches

$$U^* = \sigma^* \varepsilon^* + \tau^* \gamma^* \tag{1}$$

where the two terms cover both normal and shear stresses. As a practical implementation of this criterion, one may, for example,

replace the irregular area under the curve in Fig. 1 by a rectangular one with ordinate σ^* equaling the average maximum stress, and a corresponding value for the abscissa equaling ε^*. An alternate form of Eq. (1) may be written as a strength criterion:

$$\left(\sigma_n/\sigma^*\right)^2 + \left(\sigma_s/\tau^*\right)^2 \leq C \tag{2}$$

where σ_n and σ_s are the actual normal and shear stresses and σ^*, τ^*, and C are values determined from tests on pure stress states as in Fig. 1. The criterion of Eq. (1) or Eq. (2) is essentially the same as the maximum total energy criterion, which has been proposed by Beltrami and Haigh (see Ref. 8) for linear materials with well-defined yield points. Herein, the total energy criterion is extended to the nonlinear Velcro behavior.

Numerical Simulation of Velcro-Controlled Deployment

Finite Element Model of Velcro Surface

In this section, interaction between Velcro and the host membrane inflatable structures is simulated numerically using a simple Velcro model consistent with the finite element approach. In this model, a two-layer Velcro is modeled by two layers of membrane elements. Elements of the same layer share common nodes having three degrees of freedom only, assuming negligible bending stiffness of the assembly. The schematic in Fig. 5 shows a typical model of Velcro-connected membrane segment. The interlocking microstructure at the interface is simulated by a finite number of interconnections (or ties) at corresponding pairs of nodes on the two layers. Thus, two nodes across the interface from each other are constrained to move together elastically if the Velcro is interlocked at that nodal location. The elastic constraint continues at a given pair of nodes as long as Eq. (1) or Eq. (2) is satisfied there. Otherwise, the two nodes are allowed to separate and move independently. This is the Velcro–membrane interaction model to be incorporated with the deployment analysis in the next section.

Velcro-Controlled Deployment

Velcro-controlled deployment of inflatables is modeled using the finite element Velcro–membrane interaction model outlined in the preceding section, along with the finite volume inflation approach.[9] In this latter approach, a cylindrical inflatable tube is simulated in its stowed configuration by a set of interconnected finite volumes (enclosures) formed by membrane elements (Fig. 6). The gas flow

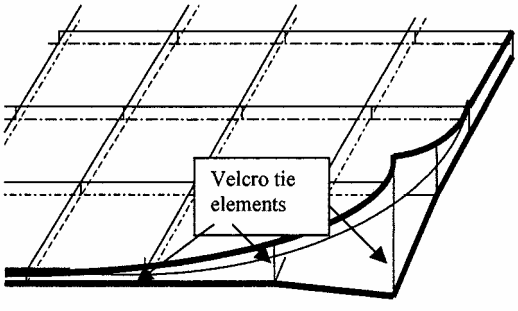

Fig. 5 Finite element idealization of Velcro-connected membrane segment.

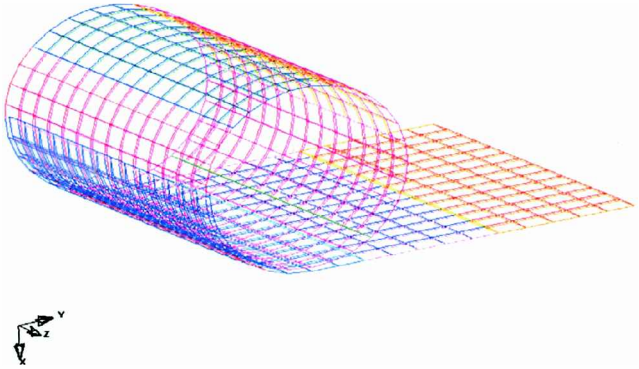

Fig. 6 Finite volume model of Velcro-controlled deployment of rolled tube.

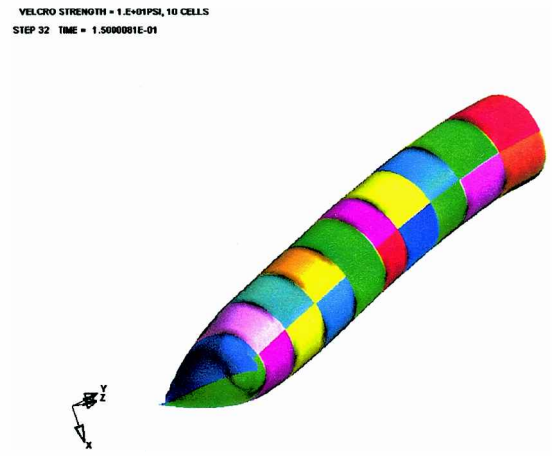

Fig. 7a Fully deployed tube with 10-psi (6.894*e*+04-Pa) Velcro.

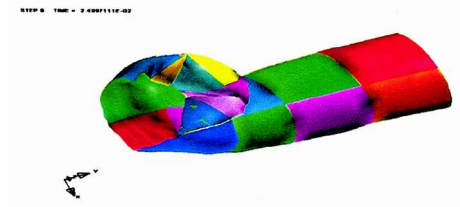

Fig. 7b Firmly interlocked tube with 10,000-psi (6.894*e*+07-Pa) Velcro.

is discretized by allowing the finite volumes to vent to each other through artificial orifices, whose areas are functions of the state of inflation. In the rolled configuration of Fig. 6, 10 finite volumes are used, each of which is defined by a much finer mesh of membrane elements. Velcro attachment is placed on the interfacing sides of 90-deg overlapping arc segments. Initially, the Velcro is assumed completely interlocked. As inflation progresses, the Velcro will debond, and separation will progressively take place. This is implemented in DYNA3D with the tie-break algorithm, in which the "tie" constraining a pair of nodes i and j on the mating interfaces will break when the normal and shear stresses σ_n and σ_s at the tie satisfy the condition of Eq. (2).

Simulation of the Velcro-controlled deployment of the rolled tube was performed for several cases in which the Velcro strength ($\sigma^* = \tau^*$) assumed values from 1 to 10,000 psi (6.894*e*+03 to 6.894*e*+07 Pa). For all cases, inflation is achieved by specifying the same rate of gas flow as a function of time. Complete inflation and Velcro separation occurred as long as ($\sigma^* = \tau^*$) < 1000 psi (6.894*e*+06 Pa). Figures 7a and 7b compare a fully inflated tube with Velcro strength $\sigma^* = \tau^* = 10$ psi (6.894*e*+04 Pa) and the same case with $\sigma^* = \tau^* = 10{,}000$ psi (6.894*e*+07 Pa). The latter, with arbitrarily high Velcro strength, remained firmly interlocked and could not deploy fully.

Whereas it is essential to determine whether a selected type of Velcro will deploy, it is of equal interest to the designer to assess the rate of deployment. Clearly, the rate of deployment is a function of several parameters that include the Velcro strength, as well as the geometric configuration of the inflatable component itself. Thus, no generalized relationship is possible. Instead, we look for sensitive indicators that could help the analyst/designer in selecting the Velcro strength for a particular inflatable membrane structure. Several such indicators are examined next.

First, as is evident from Figs. 8a and 8b, the time histories of the inflated volume for the same two cases [$\sigma^* = \tau^* = 10$ psi (6.894*e*+04 Pa) and 10,000 psi (6.894*e*+07 Pa)] do not seem to be sensitive to variability in the rate of deployment. Rather, they seem to indicate merely the degree of inflation. Second, consider the displacement-time history examples shown in Figs. 9a and 9b for two corresponding interface nodes. Figure 9a is for $\sigma^* = \tau^* = 10$ psi (6.894*e*+04 Pa), which is typical of other cases where complete separation and deployment occurred. Figure 9b is for $\sigma^* = \tau^* = 10{,}000$ psi (6.894*e*+07 Pa), where Velcro separation

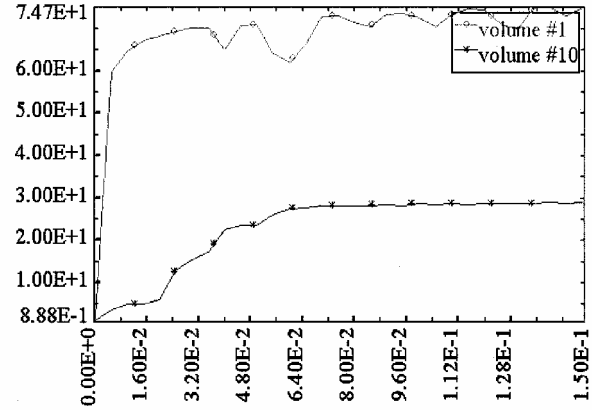

Fig. 8a Time history of inflated volume under 10 psi (6.894*e*+04 Pa).

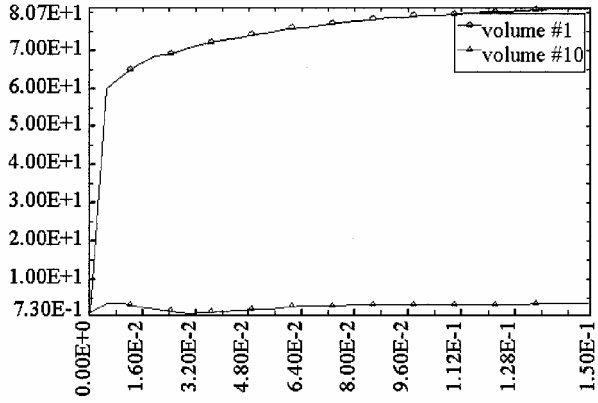

Fig. 8b Time history of inflated volume under 10,000-psi (6.894*e*+07-Pa) Velcro.

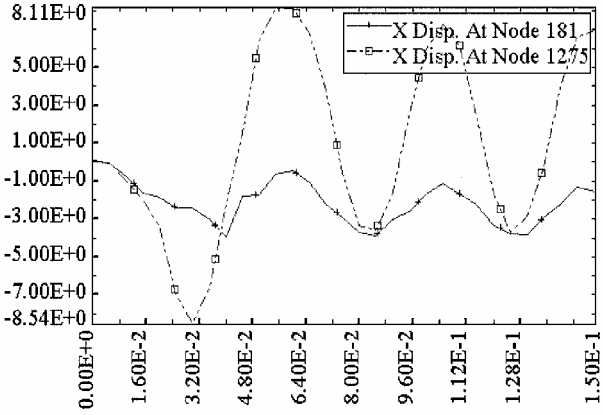

Fig. 9a Displacement history of two nodes tied by 10-psi (6.894*e*+04-Pa) Velcro.

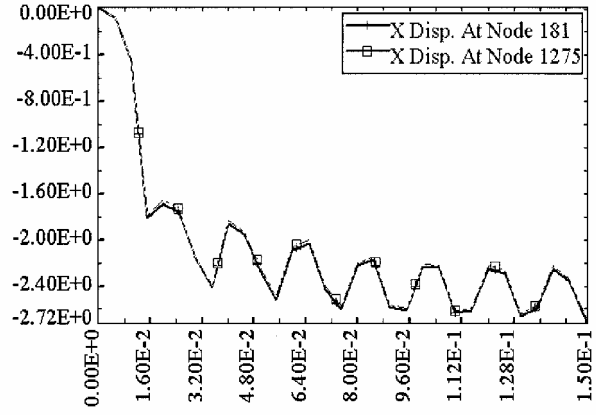

Fig. 9b Displacement history of two nodes tied by 10,000-psi (6.894*e*+07-Pa) Velcro.

Table 2 Rate of energy dissipation along the interface of Velcro with different strengths

$\sigma^* = \tau^*$ psi (Pa)	ΔE_i/in.^{2} (J/m^2)
1 (6.894+03)	1 (175.12)
5 (3.447+04)	1.5 (262.68)
10 (6.894+04)	1.875 (328.35)
100 (6.894+05)	5 (875.59)
1,000 (6.894+06)	25 (4,377.95)
10,000 (6.894+07)	250 (43,779.5)

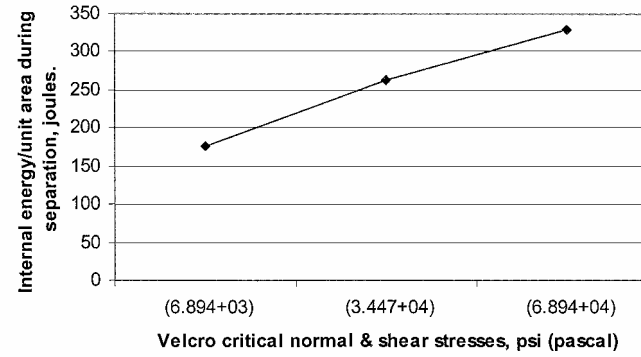

Fig. 10 Rate of energy dissipation along Velcro interface as function of Velcro strength.

never took place. From this type of data, one can compute the relative displacement between nodes at the Velcro interface as a direct indicator of degree and rate of deployment. However, selecting which nodes to use is not straightforward because Velcro separation can begin at different fronts depending on the inflatable configuration. Even for the same configuration, the Velcro with $\sigma^* = \tau^* = 1.0$ psi (6.894*e*+03 Pa) was found to separate at the leading edge of the segment, whereas the Velcro with $\sigma^* = \tau^* = 10$ (6.894*e*+04 Pa) was found to separate at the trailing edge. Such variability can be attributed to the strong nonlinearity of the problem, both because of inflation as well as because of Velcro nonlinearities.

As a third alternative, the time measured from initial inflation until Velcro begins to separate may reflect the Velcro strength, but not the rate of deployment.

Perhaps the best measure of the rate of deployment during separation is the rate of energy dissipation per unit area (ΔE_i/area) of the Velcro interfaces. This criterion is also consistent in spirit with the Velcro strength criterion of Eq. (1). In Table 2, we summarize numerical values of the rate of energy dissipation calculated as an average value over the entire Velcro segment for six different Velcro strengths. These are also graphed in Fig. 10 for cases with low Velcro strengths suitable for membrane structures.

Conclusions

Velcro joining has been recognized as an ideal means of limiting possible undesirable dynamics during the deployment of inflatables. This motivated the present work, which shows the following: 1) In contrast to adhesive joints, Velcro joints are highly nonlinear; they rely on multiple mechanisms that are brought to bear sequentially to resist separation. 2) To best capture the unique Velcro behavior, the strain energy strength criterion is proposed to predict separation in Velcro. When applied to Velcro separation in peeling tests, the criterion was consistent with the trend in variations in the peeling load. 3) Although it is essential to determine whether a selected type of Velcro will deploy, it is of equal interest to the designer to assess the rate of deployment. As a suitable measure for selecting a particular Velcro strength for a particular inflatable configuration, we propose the rate of interface energy dissipation as a sensitive indicator of the rate of deployment.

Acknowledgments

This research was performed at the Jet Propulsion Laboratory, California Institute of Technology, under contract with NASA. Funding was provided by NASA's Cross Enterprise Technology

Development. Our special thanks to O. Quijano and J. Rodriguez of California State University at Los Angeles for performing the Velcro tests and to J. Hah of CES, Inc., for the Velcro peeling simulations.

References

[1]Lou, M., and Feria, V. A., "Controlled Deployment of Inflatable Structures," Jet Propulsion Lab., California Inst. of Technology New Technology Rept., NTR 20112/9750, Pasadena, CA, Dec. 1996.

[2]Lou, M., and Feria, V. A., "Development of Space Inflatable/Rigidizable Structures Technology," Symposium on Deployable Structures: Theory and Applications, International Union of Theoretical and Applied Mechanics, International Society for Shell and Spatial Structures, and British National Space Centre, Sept. 1998.

[3]Spies, G., "The Peel Test on Redux-Bonded Joints," *Journal of Aircraft Engineering*, Vol. 25, No. 64, 1953.

[4]Salama, M., Rowe, W., and Yasui, R., "Stress Analysis of Silicon Solar Cell Arrays and Related Material Properties," Jet Propulsion Lab., California Inst. of Technology, TR 32-1552, Pasadena, CA, March 1972.

[5]Kim, K.-S., and Aravas, N., "Elasto-Plastic Analysis of the Peel Test," *International Journal of Solids and Structures*, Vol. 24, No. 4, 1988, pp. 417–435.

[6]Nayeb-Hashemi, H., and Jawad, O. C., "Theoretical and Experimental Evaluation of the Bond Strength Under Peeling Loads," *Journal of Engineering Materials and Technology*, Vol. 119, 1997, pp. 415–421.

[7]Park, I. S., Yu, J., and Park, Y. B., "Peel Strength in the Cu/Cr/Polyimide System," *Materials Research Society Symposium Proceedings*, Vol. 436, 1997, pp. 133–138.

[8]Timoshenko, S., *Strength of Materials—Part II: Advanced Theory and Problems*, 3rd ed., reprint, Van Nostrand, Princeton, NJ, 1963.

[9]Salama, M., Kuo, C. P., and Lou, M., "Simulation of Deployment Dynamics of Inflatable Structures," *AIAA Journal*, Vol. 38, No. 12, 2000, pp. 2277–2283.

J. Lassiter
Guest Editor